




Changes in frontal aslant tract tractography in selected types of brain tumours

Sara Kierońska-Siwak¹ , Magdalena Jabłońska², Paweł Sokal¹

¹Department of Neurosurgery and Neurology, Jan Bizioł University Hospital No. 2, Collegium Medicum of Nicolaus Copernicus University, Bydgoszcz, Poland

²Doctoral School of Medical and Health Sciences, Collegium Medicum, Nicolaus Copernicus University, Bydgoszcz, Poland

ABSTRACT

Aim of the study. To present differences in frontal aslant tract (FAT) tractography among patients diagnosed with primary brain tumours and metastatic brain tumours.

Material and methods. The analysis included 38 patients diagnosed with a frontal brain tumour. A control group of 30 healthy patients was also considered. The FAT was delineated, taking into account ROI 1 — the superior frontal gyrus, and ROI 2 — SMA. Endpoints were determined on the pars opercularis and pars triangularis of the inferior frontal gyrus. FAT was delineated in four different ways for each patient.

Results. In the group of patients with a brain tumour, a lower volume of FAT and a reduced quantity of fibres were observed compared to the control group. Comparison of the examined parameters between patients with glioblastoma and metastasis revealed statistically significant differences for MD ($p < 0.001$) regardless of the selected projection.

Conclusions. The difference in MD (mean diffusivity) among patients with metastatic tumours may be related to an increased oedema zone.

Keywords: tractography, DTI, FAT, brain tumour

(*Neurol Neurochir Pol* 2024; 58 (1): 106–111)

Introduction

The frontal aslant tract (FAT) is a short fibre tract predominantly located in the left hemisphere, first described by Catani in 2012. It connects the superior frontal gyrus (SFG) with the inferior frontal gyrus (IFG) and supplementary motor area (SMA). Extensive analysis of the fibre course, fMRI findings, and direct cortical stimulation have demonstrated a significant role played by the FAT in speech processing [1].

The role of the FAT extends beyond mere connectivity, as it serves as a critical connection between motor planning, initiation, and language control. FAT is involved in various

language functions, particularly speech production and language control. The pre-SMA, connected to the IFG through the FAT, plays a role in several aspects of language processing, such as articulatory planning and control. Conversely, the IFG plays a vital role in language production, speech fluency, and language control processes [2].

The FAT facilitates the transformation of linguistic intentions into motor plans, ensuring the seamless execution of speech production [3].

Despite the growing interest and an increase in publications on the FAT, there remains limited knowledge about this white matter bundle in clinical practice. FAT exhibits

Address for correspondence: Sara Kierońska-Siwak, Department of Neurosurgery and Neurology, Jan Bizioł University Hospital No. 2, Collegium Medicum of Nicolaus Copernicus University, Ujejskiego 75 St., 85–168 Bydgoszcz, Poland; e-mail: sara.kieronska@gmail.com

Received: 07.11.2023 Accepted: 19.12.2023 Early publication date: 17.01.2024

This article is available in open access under Creative Common Attribution-Non-Commercial-No Derivatives 4.0 International (CC BY-NC-ND 4.0) license, allowing to download articles and share them with others as long as they credit the authors and the publisher, but without permission to change them in any way or use them commercially.

connections to the upper frontal lobe, lower frontal lobe, SMA, and pre-SMA. Damage to these white matter connections can have more significant clinical effects compared to damage to the cerebral cortex. This is because the consequences of cortical damage can be mitigated over time due to the high plasticity of the cortex [4].

Therefore, and due to the numerous functions performed by the FAT, there is a need to share knowledge about the anatomy of the SMA region and related white matter pathways. This subject should be particularly well understood, especially in the case of frontal lobe tumour surgery [5].

The aim of this study was to present the anatomical variability of the FAT, with a particular emphasis on demonstrating the length and volume of the pathway based on the chosen region of interest (ROI).

Material and methods

Patients treated for frontal lobe tumours at a single institution were retrospectively reviewed. A total of 38 adult patients (20 males, 18 females) who underwent resection surgery at the Neurosurgery and Neurology Department of Jan Biziel University Hospital in Bydgoszcz, Poland (blinded for peer review purposes) between 2020 and 2022 were included in the study. The mean age in the treated group was 56.93 ± 15.46 years. The mean standard volume of the tumour was $3.517\text{cc} \pm 2.227\text{cc}$.

The study focused on patients diagnosed with a brain tumour involving the frontal lobe. Among them, 17 patients had a tumour affecting the right frontal lobe, while 21 patients had a tumour affecting the left frontal lobe. All patients underwent surgical treatment.

MRI and DTI acquisition

In this study, MRI and DTI acquisition parameters similar to those previously developed by the authors in other publications were used. This is because all investigations in this study, as well as in the authors' previous publications, were conducted using the same MRI scanner, and tractography was generated using the same software (DSI studio). Therefore, the methodology section in the article has already been published.

All patients underwent imaging at 3.0 T using a Philips Ingenia scanner manufactured in 2015 and a 32-channel head coil. The head was scanned without any angulation, with an angle of 0° in all directions (AP, RL, FH).

A deterministic fibre tracking method was used with a DTI diffusion scheme and a total of 60 diffusion sampling directions. The in-plane resolution was 1.87514 mm, and the slice thickness was 2 mm. The angular threshold for fibre tracking was set at 60 degrees. Regions of interest were automatically defined based on an anatomical atlas loaded into the DSI Studio program (<http://dsi-studio.labsolver.org>) [6–8].

Statistical analysis

The statistical analysis was performed using Statistica 13 software. The Shapiro-Wilk test was used to assess the normal distribution of qualitative data. Parametric tests, such as Student's t-test for dependent and independent variables, and Pearson's rank correlation test, were employed if the data exhibited normal distribution.

For data that did not follow a normal distribution, non-parametric tests were used. The Mann-Whitney test was used for group comparisons, the Wilcoxon test for dependent variables, and the Spearman's rank correlation test for analysing correlations. A significance level of $p < 0.05$ was considered for all analyses.

DTI analysis

All analysis of images was provided using DSI Studio software (dsistudio.labsolver.org, BSD License.). The anisotropy threshold was determined automatically by the software. A total of 15,000 tracts were calculated. When reconstructing the FAT, we obtained tract statistics, including the number of tracks, the mean length, and the volume of the FAT [8].

Fibre tracking

We reconstructed the FAT based on ROIs: ROI 1 - gyrus frontalis superior (SFG) and ROI 2 - SMA. End points were based on pars opercularis of gyrus frontalis inferior (IFG-op) and pars triangularis of gyrus frontalis inferior (IFG-tri).

Start points were designated as: SFG and SMA. The end points were based on: gyrus frontalis inferior pars triangularis (IFG-tri) and gyrus frontalis inferior pars opercularis (IFG-op). By mixing and matching start and end points, we obtained FAT for analysis by four different types in each patient (Fig. 1).

Results

The FAT was reconstructed using four different algorithms for each patient in the study.

Among the 38 patients, 14 were diagnosed with primary tumours, specifically glioblastoma multiforme WHO IV (eight patients IDH-mutant, and six patients IDH wildtype), and five patients had astrocytoma anaplasticum WHO III. Additionally, 19 patients had metastatic tumours, including 10 with lung cancer metastasis, six with colorectal cancer, and three with melanoma.

Comparisons of fractional anisotropy (FA) and mean diffusivity (MD) in both groups are set out in Table 1.

In the study group, the number of fibres and volume of FAT were lower than in the control group, regardless of the chosen method for FAT plotting. Additionally, a significant statistical difference ($p < 0.05$) in the number of fibres was identified between patients in the control and study groups, in each of the selected projections. Regarding the volume of the tract, statistical significance was achieved in the SMA-IFG

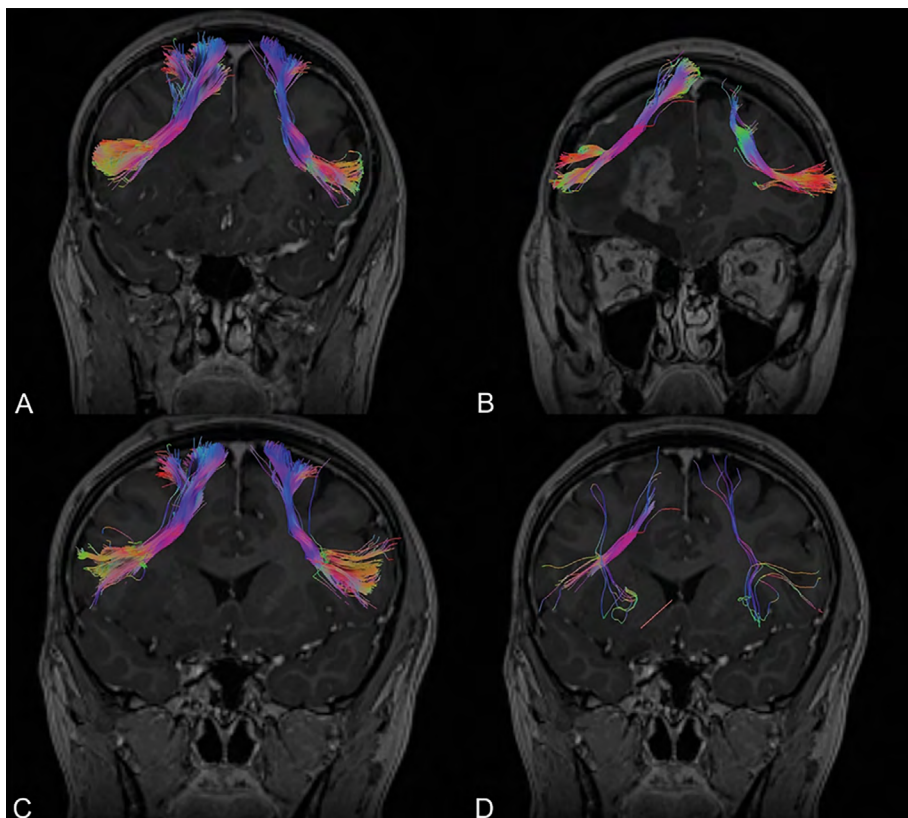


Figure 1. Frontal aslant tract (FAT); **A.** ROI 1 – gyrus frontalis superior with end point-pars opercularis of gyrus frontalis inferior (IPG-op), **B.** ROI 1 with end point-pars triangularis of gyrus frontalis inferior (IPG-tri), **C.** ROI 2 – SMA with IPG-op, **D.** ROI 2 with IPG-tri

Table 1. Comparison of FA and MD values in study and control groups depending on region of interest and endpoints

	MD study group			MD control group			p-value	FA study group			FA control group			p-value
	SD	Me		SD	Me			SD	Me		SD	Me		
SFG-IFGop	0.77	0.13	0.72	0.49	0.06	0.50	< 0.001	0.42	0.05	0.42	0.69	0.09	0.69	< 0.001
SFG-IFG tra	0.78	0.09	0.77	0.48	0.07	0.49	< 0.001	0.42	0.04	0.42	0.74	0.06	0.74	< 0.001
SMA-IFGop	0.75	0.09	0.72	0.48	0.07	0.49	< 0.001	0.44	0.05	0.46	0.76	0.07	0.78	< 0.001
SMA-IFG tra	0.77	0.06	0.79	0.47	0.08	0.49	< 0.001	0.46	0.06	0.46	0.76	0.07	0.79	< 0.001

MD — mean diffusivity; FA — fractional anisotropy; SD — standard deviation; Me — median; SFG — superior frontal gyrus; IFG — inferior frontal gyrus; SMA — supplementary motor area

tri projection ($p < 0.001$; 464.8 ± 92.5 vs. 632.3 ± 89.6 ; study group vs. control group), SMA-IFG op projection ($p < 0.001$; $2,738.3 \pm 1,374.7$ vs. $5,028.3 \pm 1,238.1$; study group vs. control group), and SFG-IFG op projection ($p < 0.001$; $40,806.7 \pm 9,284.5$ vs. $52,831.7 \pm 2,399.0$; study group vs. control group). However, in terms of fibre length, the threshold of statistical significance was reached only in the SMA-IFG projection ($p = 0.045$; 81.8 ± 6.4 vs. 86.5 ± 5.7 ; study group vs. control group).

Comparison of the examined parameters between patients with glioblastoma and metastasis revealed statistically significant differences for MD ($p < 0.001$) regardless of the selected projection. The specific values are set out in Table 2. However, no statistically significant differences were found for the remaining parameters in the projections used, except for the SMA-IFG op projection. In this projection, statistically significant differences were also identified in the number of fibres ($p = 0.028$; 179.6 ± 90.0 vs. 304.6 ± 106.5 ; glioblastoma vs.

Table 2. Comparison of FA and MD values depending on regions of interest and endpoints in group of patients with primary tumours and metastases

	MD GBM group			MD metastasis group			p-value	FA GBM group		FA metastasis group		p-value		
	SD	Me		SD	Me			SD	Me	SD	Me			
SFG-IFGop	0.66	0.04	0.67	0.89	0.05	0.89	< 0.001	0.42	0.06	0.41	0.42	0.03	0.42	0.985
SFG-IFG tra	0.70	0.03	0.70	0.86	0.05	0.84	< 0.001	0.42	0.04	0.43	0.42	0.03	0.41	0.874
SMA-IFGop	0.68	0.04	0.69	0.84	0.04	0.82	< 0.001	0.44	0.06	0.43	0.45	0.03	0.46	0.862
SMA-IFG tra	0.72	0.04	0.71	0.82	0.03	0.82	< 0.001	0.46	0.08	0.45	0.46	0.03	0.46	0.875

MD — mean diffusivity; FA — fractional anisotropy; SD — standard deviation; Me — median; SFG — superior frontal gyrus; GBM — glioblastoma; IFG — inferior frontal gyrus; SMA — supplementary motor area

metastasis) and tract volume ($p = 0.032$; $2,040.8 \pm 1,042.0$ vs. $3,535.4 \pm 1,323.9$; glioblastoma vs. metastasis).

Based on analysis of the results obtained in the group of cancer patients, statistically significant differences ($p < 0.05$) were observed between the results recorded in the SFG-IFG op and SMA-IFG op ROIs for the parameters related to the number of fibres ($p < 0.001$; $1,548.5 \pm 397.1$ vs. 237.9 ± 114.3 ; SFG vs. SMA) and the tract volume ($p < 0.001$; $40,806.7 \pm 9,284.5$ vs. $2,738.3 \pm 1,374.7$; SFG vs. SMA). However, the parameters MD, FA, and fibre length did not reach the level of statistical significance. A strong positive correlation was identified for MD using Pearson's rank correlation test ($0.9 < R < 1.0$), and this reached statistical significance ($p < 0.001$).

In the same group, when analysing data obtained in the SFG-IFG tra vs. SMA-IFG tra ROIs, statistical significance ($p < 0.05$) was observed for the number of fibres ($p < 0.001$; 470.1 ± 106.8 vs. 24.8 ± 11.0 ; SFG vs. SMA) and the tract volume ($p = 0.001$; $6,288.5 \pm 3,790.3$ vs. 464.8 ± 92.5 ; SFG vs. SMA), as well as for fibre length ($p = 0.008$; 91.41 ± 3.92 vs. 87.18 ± 6.544 ; SFG vs. SMA) and FA ($p = 0.037$; 0.42 ± 0.004 vs. 0.46 ± 0.006 ; SFG vs. SMA). However, MD and fibre length analysis results in the above ROIs did not reach statistical significance. Additionally, two statistically significant ($p < 0.05$) positive correlations were identified for fibre length ($p = 0.022$) and MD ($p < 0.001$).

Discussion

In this study, we employed DTI diffusion tractography as a valuable non-invasive technique for mapping white matter fibres in patients with brain tumours [9, 10]. This method plays a critical role in surgical planning, allowing for a balance between radical tumour resection and the preservation of neuronal functions [11, 12]. However, DTI has limitations that can impact the quality of white matter fibre visualisation. Factors such as reduced fractional anisotropy (FA), mass effect, tumour infiltration, neoplastic vascular oedema, and destruction of white matter tracts can disrupt the spatial orientation of fibres and alter the direction of water diffusion, thereby affecting the effectiveness of the technique [13–16].

DTI has shown promise in the differential diagnosis of glioblastoma and metastatic tumours, but consistent data from independent studies is lacking [17]. Our results comparing glioblastoma and metastatic tumours demonstrated a statistically significant difference in the MD parameter across all four projections, with higher average diffusivity values observed in metastatic tumours [17].

These findings differ from the existing literature, highlighting the lack of consensus regarding DTI metrics when comparing glioblastoma and metastatic tumours [18–20]. Byrnes et al. [21] reported higher MD values in the glioblastoma area, with even higher values in the tissue surrounding the metastasis compared to the peri-glioblastoma region.

In our study, we did not find statistically significant differences in the FA parameter between patients with glioblastoma and metastases. Moreover, the values obtained were practically identical, regardless of the defined fibre assignment by continuous tracking (FAT) projections. This result may be attributable to the small sample size in our study. However, existing literature suggests higher FA values in glioblastoma compared to metastatic tumours [22–24]. The FA parameter reflects water diffusion direction for each voxel, determining the degree of anisotropy in the studied structure [25]. Several variables, such as fibre structural integrity, packing density, myelination degree, and fibre diameter, significantly influence this parameter [26–28]. Wang et al. [29] proposed that the increase in fractional anisotropy in glioblastoma might be related to the spatial orientation of the tumour-overproduced extracellular matrix infiltrating adjacent healthy tissue, suggesting a relationship between scalar values and cell orientation in the imaged voxel. These authors also reported significantly higher FA values in glioblastoma compared to metastatic tumours, and did not find statistically significant differences in the MD parameter between the two. However, there is a lack of consistency in the available literature regarding FA and MD parameters. For instance, Wang et al. [29] and Reiche et al. [30] reported lower fractional anisotropy in gliomas compared to brain metastases.

The heterogeneity of results obtained in subsequent studies may be attributed to differences in the choice of techniques for

defining the ROI, and the small size of patient groups. Various hypotheses have been proposed to explain the inconsistency of results. Reiche et al. [30] suggested that discrepancies arise from the inclusion of different tumour areas in the study. The solid part of the tumour, which corresponds to the enhanced area, contains fibres that have been damaged or displaced by tumour expansion. On the other hand, the non-enhanced area consists of both solid tumour tissue and remnants of white matter fibres, which can result in increased FA values [30–32]. On the other hand, Wang et al. [29] suggested that higher FA values result from increased cellularity in glioblastoma compared to metastasis, leading to a reduction in extracellular space volume and an increase in water diffusion directivity [31].

Higher FA values have also been associated with highly differentiated brain tumours, along with lower MD values compared to intracranial metastases, probably due to differences in tumour structure organisation [32]. However, even in this case, the data on DTI metrics for differentiating high-grade gliomas from metastases is inconsistent [33].

It is important to consider that developing tumours impact upon surrounding tissues, resulting in changes such as vascular oedema and fibre infiltration, sometimes leading to damage [14–16]. These changes are reflected in FA and MD values. Byrnes et al. [21] demonstrated significant differences in these parameters in the oedema area surrounding glioblastoma and metastases. MD was significantly higher, and FA was significantly reduced, in the oedema surrounding metastases compared to oedema around glioblastoma multiforme. Additionally, the glioblastoma area showed significantly higher MD. Based on these findings, the authors concluded that simultaneous determination of DTI metrics in both the tumour area and adjacent peritumoural tissue could serve as a reliable tool for differentiating glioblastoma from intracranial metastasis. Lu et al. [34] suggested that lower FA values in the tissue around glioblastoma are a consequence of the destructive effect of tumour-derived cells on white matter fibres.

Furthermore, it should be considered whether the histological type of intratumoural metastasis may influence DTI parameters in the surrounding tissue.

During our analysis, we observed a statistically significant difference in the MD parameter between metastatic tumours and primary lesions, consistently observed in each selected projection.

Another proposed explanation for the differences in FA and MD between primary tumours and metastases is the dissimilarity in the nature of oedema surrounding the lesions. Peritumoural oedema predominantly forms around metastatic tumours, leading to an increase in MD. In contrast, tumour infiltration oedema, characteristic of glioblastoma, results in lower MD values. Additionally, the FA value around the tumour does not show a significant difference for both types of lesions due to the overlapping effects of both types of oedema

to varying degrees [35]. This theory partly explains our MD results for metastatic tumours.

Conclusions

The presence of a brain tumour affects the parameters of FAT tractography, leading to a reduction in the volume of the pathway and the number of fibres within the bundle. Furthermore, we observed differences in MD depending on the type of brain tumour. The difference in tractography parameters in the study group may be associated with the tumour infiltration into the FAT and the oedematous zone around the tumour.

Article information

Data availability statement: *No experimental data or materials have been used for this review other than the published and reviewed bibliography.*

Ethics statement: *All patients signed informed consent to participate in the study. Consent for the study was issued by the local bioethics committee with the number KB 532.*

Funding: *This research received no external funding.*

Conflicts of interest: *The authors declare no conflict of interest.*

References

1. Catani M, Dell'Acqua F, Vergani F, et al. Short frontal lobe connections of the human brain. *Cortex*. 2012; 48(2): 273–291, doi: [10.1016/j.cortex.2011.12.001](https://doi.org/10.1016/j.cortex.2011.12.001), indexed in Pubmed: [22209688](https://pubmed.ncbi.nlm.nih.gov/22209688/).
2. Dick AS, Garic D, Graziano P, et al. The frontal aslant tract (FAT) and its role in speech, language and executive function. *Cortex*. 2019; 111: 148–163, doi: [10.1016/j.cortex.2018.10.015](https://doi.org/10.1016/j.cortex.2018.10.015), indexed in Pubmed: [30481666](https://pubmed.ncbi.nlm.nih.gov/30481666/).
3. Aron AR, Behrens TE, Smith S, et al. Triangulating a cognitive control network using diffusion-weighted magnetic resonance imaging (MRI) and functional MRI. *J Neurosci*. 2007; 27(14): 3743–3752, doi: [10.1523/JNEUROSCI.0519-07.2007](https://doi.org/10.1523/JNEUROSCI.0519-07.2007), indexed in Pubmed: [17409238](https://pubmed.ncbi.nlm.nih.gov/17409238/).
4. La Corte E, Eldahaby D, Greco E, et al. The frontal aslant tract: a systematic review for neurosurgical applications. *Front Neurol*. 2021; 12: 641586, doi: [10.3389/fneur.2021.641586](https://doi.org/10.3389/fneur.2021.641586), indexed in Pubmed: [33732210](https://pubmed.ncbi.nlm.nih.gov/33732210/).
5. Burkhardt E, Kinoshita M, Herbet G. Functional anatomy of the frontal aslant tract and surgical perspectives. *J Neurosurg Sci*. 2021; 65(6): 566–580, doi: [10.23736/S0390-5616.21.05344-3](https://doi.org/10.23736/S0390-5616.21.05344-3), indexed in Pubmed: [33870673](https://pubmed.ncbi.nlm.nih.gov/33870673/).
6. Szmuda T, Kierońska S, Ali S, et al. Tractography-guided surgery of brain tumours: what is the best method to outline the corticospinal tract? *Folia Morphol (Warsz)*. 2021; 80(1): 40–46, doi: [10.5603/FM.a2020.0016](https://doi.org/10.5603/FM.a2020.0016), indexed in Pubmed: [32073136](https://pubmed.ncbi.nlm.nih.gov/32073136/).

7. Kierońska-Siwak S, Sokal P, Jabłońska M, et al. Structural connectivity reorganization based on DTI after cingulotomy in obsessive-compulsive disorder. *Brain Sci.* 2022; 13(1), doi: [10.3390/brain-sci13010044](https://doi.org/10.3390/brain-sci13010044), indexed in Pubmed: [36672026](https://pubmed.ncbi.nlm.nih.gov/36672026/).
8. Kierońska S, Sokal P, Dura M, et al. Tractography-Based analysis of morphological and anatomical characteristics of the uncinate fasciculus in human brains. *Brain Sci.* 2020; 10(10): 709, doi: [10.3390/brainsci10100709](https://doi.org/10.3390/brainsci10100709), indexed in Pubmed: [33036125](https://pubmed.ncbi.nlm.nih.gov/33036125/).
9. Jones DK, Cercignani M. Twenty-five pitfalls in the analysis of diffusion MRI data. *NMR Biomed.* 2010; 23(7): 803–820, doi: [10.1002/nbm.1543](https://doi.org/10.1002/nbm.1543), indexed in Pubmed: [20886566](https://pubmed.ncbi.nlm.nih.gov/20886566/).
10. Farquharson S, Tournier JD, Calamante F, et al. White matter fiber tractography: why we need to move beyond DTI. *J Neurosurg.* 2013; 118(6): 1367–1377, doi: [10.3171/2013.2.JNS121294](https://doi.org/10.3171/2013.2.JNS121294), indexed in Pubmed: [23540269](https://pubmed.ncbi.nlm.nih.gov/23540269/).
11. Kierońska S, Słoniewski P. The usefulness and limitations of diffusion tensor imaging — a review study. *Eur J Transl Clin Med.* 2020; 2(2): 43–51, doi: [10.31373/ejtc/112437](https://doi.org/10.31373/ejtc/112437).
12. Dubey A, Kataria R, Sinha VD. Role of diffusion tensor imaging in brain tumor surgery. *Asian J Neurosurg.* 2018; 13(2): 302–306, doi: [10.4103/ajns.AJNS_226_16](https://doi.org/10.4103/ajns.AJNS_226_16), indexed in Pubmed: [29682025](https://pubmed.ncbi.nlm.nih.gov/29682025/).
13. Szmuda T, Kierońska S, Ali S, et al. Tractography-guided surgery of brain tumours: what is the best method to outline the corticospinal tract? *Folia Morphol (Warsz).* 2021; 80(1): 40–46, doi: [10.5603/FM.a2020.0016](https://doi.org/10.5603/FM.a2020.0016), indexed in Pubmed: [32073136](https://pubmed.ncbi.nlm.nih.gov/32073136/).
14. Alexander AL, Hasan KM, Lazar M, et al. Analysis of partial volume effects in diffusion-tensor MRI. *Magn Reson Med.* 2001; 45(5): 770–780, doi: [10.1002/mrm.1105](https://doi.org/10.1002/mrm.1105), indexed in Pubmed: [11323803](https://pubmed.ncbi.nlm.nih.gov/11323803/).
15. Provenzale JM, McGraw P, Mhatre P, et al. Peritumoral brain regions in gliomas and meningiomas: investigation with isotropic diffusion-weighted MR imaging and diffusion-tensor MR imaging. *Radiology.* 2004; 232(2): 451–460, doi: [10.1148/radiol.2322030959](https://doi.org/10.1148/radiol.2322030959), indexed in Pubmed: [15215555](https://pubmed.ncbi.nlm.nih.gov/15215555/).
16. Abhinav K, Yeh FC, Pathak S, et al. Advanced diffusion MRI fiber tracking in neurosurgical and neurodegenerative disorders and neuroanatomical studies: a review. *Biochim Biophys Acta.* 2014; 1842(11): 2286–2297, doi: [10.1016/j.bbadis.2014.08.002](https://doi.org/10.1016/j.bbadis.2014.08.002), indexed in Pubmed: [25127851](https://pubmed.ncbi.nlm.nih.gov/25127851/).
17. Jiang R, Du FZ, He Ci, et al. The value of diffusion tensor imaging in differentiating high-grade gliomas from brain metastases: a systematic review and meta-analysis. *PLoS One.* 2014; 9(11): e112550, doi: [10.1371/journal.pone.0112550](https://doi.org/10.1371/journal.pone.0112550), indexed in Pubmed [25380185](https://pubmed.ncbi.nlm.nih.gov/25380185/).
18. Sternberg EJ, Lipton ML, Burns J. Utility of diffusion tensor imaging in evaluation of the peritumoral region in patients with primary and metastatic brain tumors. *AJNR Am J Neuroradiol.* 2014; 35(3): 439–444, doi: [10.3174/ajnr.A3702](https://doi.org/10.3174/ajnr.A3702), indexed in Pubmed: [24052506](https://pubmed.ncbi.nlm.nih.gov/24052506/).
19. Fordham AJ, Hachert CC, Patel N, et al. Differentiating glioblastomas from solitary brain metastases: an update on the current literature of advanced imaging modalities. *Cancers (Basel).* 2021; 13(12): 2960, doi: [10.3390/cancers13122960](https://doi.org/10.3390/cancers13122960), indexed in Pubmed: [34199151](https://pubmed.ncbi.nlm.nih.gov/34199151/).
20. Yeh FC, Irimia A, Bastos DC, et al. Tractography methods and findings in brain tumors and traumatic brain injury. *Neuroimage.* 2021; 245: 118651, doi: [10.1016/j.neuroimage.2021.118651](https://doi.org/10.1016/j.neuroimage.2021.118651), indexed in Pubmed: [34673247](https://pubmed.ncbi.nlm.nih.gov/34673247/).
21. Byrnes TJD, Barrick TR, Bell BA, et al. Diffusion tensor imaging discriminates between glioblastoma and cerebral metastases in vivo. *NMR Biomed.* 2011; 24(1): 54–60, doi: [10.1002/nbm.1555](https://doi.org/10.1002/nbm.1555), indexed in Pubmed: [20665905](https://pubmed.ncbi.nlm.nih.gov/20665905/).
22. Bauer AH, Ery W, Moser FG, et al. Differentiation of solitary brain metastasis from glioblastoma multiforme: a predictive multiparametric approach using combined MR diffusion and perfusion. *Neuroradiology.* 2015; 57(7): 697–703, doi: [10.1007/s00234-015-1524-6](https://doi.org/10.1007/s00234-015-1524-6), indexed in Pubmed: [25845813](https://pubmed.ncbi.nlm.nih.gov/25845813/).
23. Bette S, Huber T, Wiestler B, et al. Analysis of fractional anisotropy facilitates differentiation of glioblastoma and brain metastases in a clinical setting. *Eur J Radiol.* 2016; 85(12): 2182–2187, doi: [10.1016/j.ejrad.2016.10.002](https://doi.org/10.1016/j.ejrad.2016.10.002), indexed in Pubmed: [27842664](https://pubmed.ncbi.nlm.nih.gov/27842664/).
24. Holly KS, Barker BJ, Murcia D, et al. High-grade gliomas exhibit higher peritumoral fractional anisotropy and lower mean diffusivity than intracranial metastases. *Front Surg.* 2017; 4: 18, doi: [10.3389/fsurg.2017.00018](https://doi.org/10.3389/fsurg.2017.00018), indexed in Pubmed: [28443285](https://pubmed.ncbi.nlm.nih.gov/28443285/).
25. Beaulieu C. The basis of anisotropic water diffusion in the nervous system — a technical review. *NMR Biomed.* 2002; 15(7–8): 435–455, doi: [10.1002/nbm.782](https://doi.org/10.1002/nbm.782), indexed in Pubmed: [12489094](https://pubmed.ncbi.nlm.nih.gov/12489094/).
26. Kinoshita M, Hashimoto N, Goto T, et al. Fractional anisotropy and tumor cell density of the tumor core show positive correlation in diffusion tensor magnetic resonance imaging of malignant brain tumors. *Neuroimage.* 2008; 43(1): 29–35, doi: [10.1016/j.neuroimage.2008.06.041](https://doi.org/10.1016/j.neuroimage.2008.06.041), indexed in Pubmed: [18672074](https://pubmed.ncbi.nlm.nih.gov/18672074/).
27. Chen Y, Shi Y, Song Z. Differences in the architecture of low-grade and high-grade gliomas evaluated using fiber density index and fractional anisotropy. *J Clin Neurosci.* 2010; 17(7): 824–829, doi: [10.1016/j.jocn.2009.11.022](https://doi.org/10.1016/j.jocn.2009.11.022), indexed in Pubmed: [20427187](https://pubmed.ncbi.nlm.nih.gov/20427187/).
28. O'Donnell L, Westin CF. An introduction to diffusion tensor image analysis. *Neurosurg Clin N Am.* 2011; 22(2): 185–196, doi: [10.1016/j.nec.2010.12.004](https://doi.org/10.1016/j.nec.2010.12.004), indexed in Pubmed: [21435570](https://pubmed.ncbi.nlm.nih.gov/21435570/).
29. Wang W, Steward CE, Desmond PM. Diffusion tensor imaging in glioblastoma multiforme and brain metastases: the role of p, q, L, and fractional anisotropy. *AJNR Am J Neuroradiol.* 2009; 30(1): 203–208, doi: [10.3174/ajnr.A1303](https://doi.org/10.3174/ajnr.A1303), indexed in Pubmed: [18842762](https://pubmed.ncbi.nlm.nih.gov/18842762/).
30. Reiche W, Schuchardt V, Hagen T, et al. Differential diagnosis of intracranial ring enhancing cystic mass lesions—role of diffusion-weighted imaging (DWI) and diffusion-tensor imaging (DTI). *Clin Neurol Neurosurg.* 2010; 112(3): 218–225, doi: [10.1016/j.clineuro.2009.11.016](https://doi.org/10.1016/j.clineuro.2009.11.016), indexed in Pubmed: [20053496](https://pubmed.ncbi.nlm.nih.gov/20053496/).
31. Tsougos I, Svolos P, Kousi E, et al. Differentiation of glioblastoma multiforme from metastatic brain tumor using proton magnetic resonance spectroscopy, diffusion and perfusion metrics at 3 T. *Cancer Imaging.* 2012; 12(3): 423–436, doi: [10.1102/1470-7330.2012.0038](https://doi.org/10.1102/1470-7330.2012.0038), indexed in Pubmed: [23108208](https://pubmed.ncbi.nlm.nih.gov/23108208/).
32. Tsuchiya K, Fujikawa A, Nakajima M, et al. Differentiation between solitary brain metastasis and high-grade glioma by diffusion tensor imaging. *Br J Radiol.* 2005; 78(930): 533–537, doi: [10.1259/bjr/68749637](https://doi.org/10.1259/bjr/68749637), indexed in Pubmed: [15900059](https://pubmed.ncbi.nlm.nih.gov/15900059/).
33. Jiang R, Du FZ, He Ci, et al. The value of diffusion tensor imaging in differentiating high-grade gliomas from brain metastases: a systematic review and meta-analysis. *PLoS One.* 2014; 9(11): e112550, doi: [10.1371/journal.pone.0112550](https://doi.org/10.1371/journal.pone.0112550), indexed in Pubmed: [25380185](https://pubmed.ncbi.nlm.nih.gov/25380185/).
34. Lu S, Ahn D, Johnson G, et al. Diffusion-tensor MR imaging of intracranial neoplasia and associated peritumoral edema: introduction of the tumor infiltration index. *Radiology.* 2004; 232(1): 221–228, doi: [10.1148/radiol.2321030653](https://doi.org/10.1148/radiol.2321030653), indexed in Pubmed: [15220505](https://pubmed.ncbi.nlm.nih.gov/15220505/).
35. Lee EJ, Ahn KJ, Lee EK, et al. Potential role of advanced MRI techniques for the peritumoral region in differentiating glioblastoma multiforme and solitary metastatic lesions. *Clin Radiol.* 2013; 68(12): e689–e697, doi: [10.1016/j.crad.2013.06.021](https://doi.org/10.1016/j.crad.2013.06.021), indexed in Pubmed: [23969153](https://pubmed.ncbi.nlm.nih.gov/23969153/).